

Automated Earthmoving Status Determination

William C. Stone¹, Geraldine Cheok², and Robert Lipman³
william.stone@nist.gov, cheok@nist.gov, robert.lipman@nist.gov

ABSTRACT

Efforts are underway at the National Institute of Standards and Technology (NIST) to develop automated non-intrusive production measurement systems and procedures for monitoring the status of general earthmoving operations at typical construction sites. The approach involves the use of auto-registered Lidar range sensing systems, wireless communications, high speed networking, temporal project databases, web-based data analysis and 3D user interfaces to provide useful derivative quantities to the earthmoving contractor while at the actual construction site. These same techniques may prove useful for planning and execution of remote, autonomous excavation on other planets. Present research is focused on developing methods for automated registration of independent 2-1/2D range data, automated volumetric calculations, including cut/fill requirements and amounts of raw material removed or placed, and web-based 3D site simulators which reflect the instant terrain geometry. This paper discusses the methods employed to achieve this capability and plans currently underway for daily construction monitoring at a \$6M process plant in the spring of 2000.

Introduction

NIST is currently leading an effort to bring information technology and automation to the construction site through a joint initiative with the Construction Industry Institute (CII) known as FIATECH (for Fully Integrated and Automated Construction Technologies) [FIATECH, 1999]. Although there are many aspects to this initiative, perhaps the most novel element is the inclusion of ubiquitous, real-time (i.e. *live*) data from the construction site into the construction management process. Currently, the various AEC tasks (e.g. architectural design, structural engineering, fabrication detailing and manufacture, and construction) typically take place in a sequential fashion, often with information being transferred in the form of hardcopies or non-compatible CAD file formats. It is still common practice for fabricators to accept structural design information in digital (CAD) format and then generate their own drawings for the shop floor which ultimately are presented to the contractor as hardcopies (i.e. blueprints). Further, there are presently no means for efficiently influencing the fabrication delivery process from the construction site. For example, if a steel frame contractor's

¹ Leader, Construction Metrology and Automation Group, NIST, Gaithersburg, MD 20899/ USA

² Research Civil Engineer, Construction Metrology and Automation Group, NIST, Gaithersburg, MD 20899/ USA

³ Computer Engineer, Computer Integrated Construction Group, NIST, Gaithersburg, MD 20899/ USA

component assembly rate is set back either by bad weather or shortage of hardware, the lag times for the determination of the existence of this situation, the notification of the fabricator that a problem exists, and the response time of the fabricator, can be significant. In this case it typically means that additional laydown yard space will need to be allocated. In the reverse case the field contractor may end up waiting on materials because they were able to make better time than expected.

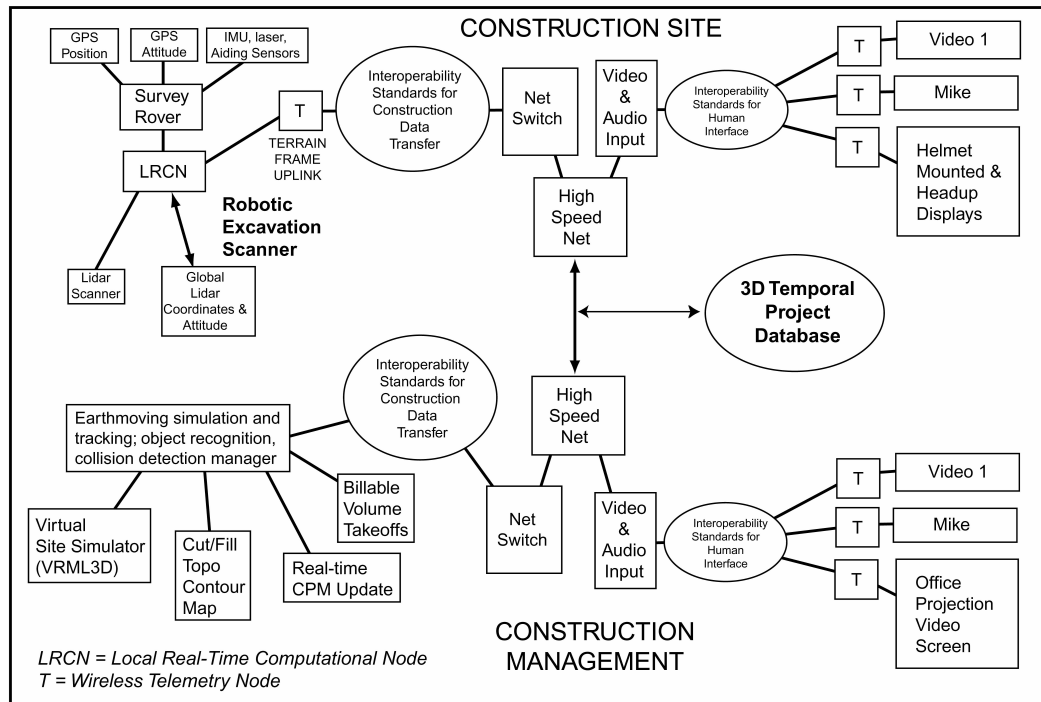


Figure 1: Network diagram for the inclusion of ubiquitous range (Lidar) sensing into the construction management process. This architecture was implemented and tested live at NIST before an audience of 300 on June 24, 1999. The audience played the role of the construction management team whose job was to assess the status of a remote construction site located one kilometer from the auditorium. Live data included audio, video, and streaming coordinate data for the survey rover. Lidar field data was uplinked following the conclusion of each scan cycle and processed at an intermediate computational node before posting for display on the construction management view screen. The NIST LiveView communications protocol provides the interoperability standard for the uplink of all these data. The data backbone consisted of a 155 Mbs ATM fiber optic link.

Through the FIATECH effort, NIST is moving to develop the infrastructure that will permit live data from the construction site to be made available to all participants in a project, including not only the direct construction management team, but also the fabricators, engineers, architects, and owners. In this paper we describe the application of FIATECH to monitoring the status of earthmoving operations. The information architecture to achieve this for excavation tracking is shown in Figure 1. We will discuss only briefly the data acquisition aspects while concentrating on the agents used to process the data that accumulates in the 3D temporal project database and to produce derivative quantities such as material removed or placed and the cut/fill requirements for the next activity cycle. For a complete description of the information technology infrastructure described in Figure 1, the reader is referred to [Cheok et.al., 1999]. Previous work on excavation automation [e.g. Krishna and Bares, 1999] focused on machinery control through localized machine-based sensors. This tends to limit the range of applicability and accuracy since line-of-sight issues restrict the field of view. The approach being taken at NIST is to develop a full-site scan from several locations on a routine basis using a robotic rover. Ultimately, a hybrid of these two approaches will no doubt be used in general earthmoving.

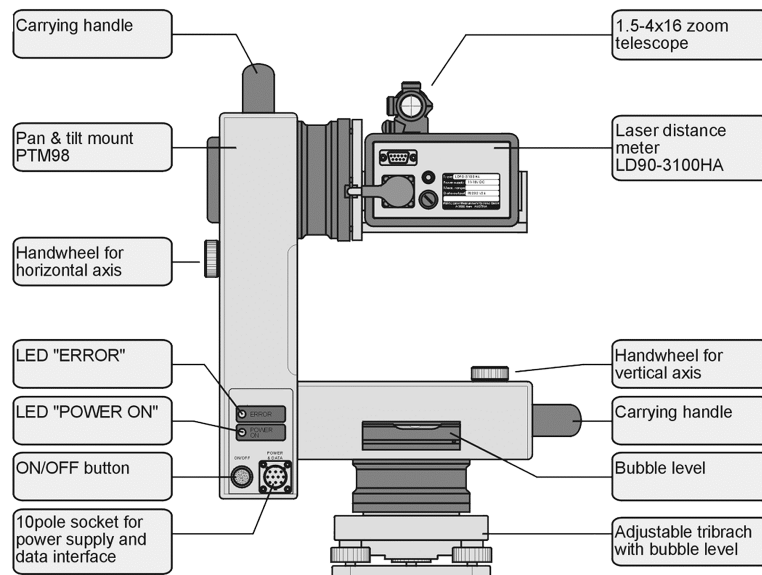


Figure 2: Lidar system used for NIST terrain modeling research. The laser is a Class 1 (eyesafe) system that emits an infrared laser pulse with a wavelength of $905 \text{ nm} \pm 5 \text{ nm}$. The measurement rate is 1 kHz. The scanning field-of-view (FOV) is $\pm 180^\circ$ horizontally and $\pm 150^\circ$ vertically. Range is 150 m for objects with reflection coefficients, r , greater than 80 % and 50 m for objects with r greater than 10 %. Distance measurements have a standard uncertainty of $\pm 20 \text{ mm}$ to $\pm 50 \text{ mm}$ (due to dust and atmospheric effects).

Terrain Acquisition

The system being developed at NIST uses a scanning Lidar (Figure 2). Work is underway presently to mount the Lidar on top of a heavily instrumented 4wd all-terrain vehicle that will register the Lidar data to the world coordinate system through real-time acquisition of the instrument frame position and attitude (using RTK GPS). A live demonstration of the system, given on June 24, 1999, was developed to illustrate the viability of using a laser scanner for terrain status assessment and the ability to wirelessly transfer data from one location to another to achieve real time progress updates at a construction site. In addition, the demonstration was used to test the effectiveness of on-the-fly post-processing tools needed to display and calculate the cut/fill requirements. For purposes of the demonstration, a small sand pile was used to simulate the terrain. The sand pile was located in the NIST Large-Scale Testing Laboratory and represented the construction site while the audience was located approximately one kilometer away in an auditorium, representing the offsite engineering office. Before the demonstration, a graphical representation of the sand pile (initial state of terrain) was created by combining Lidar-generated point clouds obtained from four locations around the sand pile. Figure 4 shows the sand pile and the four point clouds obtained by the laser scanner from around the sand pile. A laptop program, LPMScan, was used to control the laser scanner, and the data was visualized using Data Explorer [OpenDX, 1999]. The post-processing procedure, operating on an intermediate CPU located 500 m from the construction site, is described in flowchart format in Figure 3 and is described in detail at the end of this paper.

By obtaining views from different locations, a true 3-D representation of the sand pile is possible as any occluded features from one location are eliminated by the data obtained from the other locations. Prior to combining the point clouds, the data from the four locations has to be registered to a common reference frame. For the purposes of the demonstration the lidar scanning locations were previously surveyed using a total station and their relative coordinates were therefore known. The laser

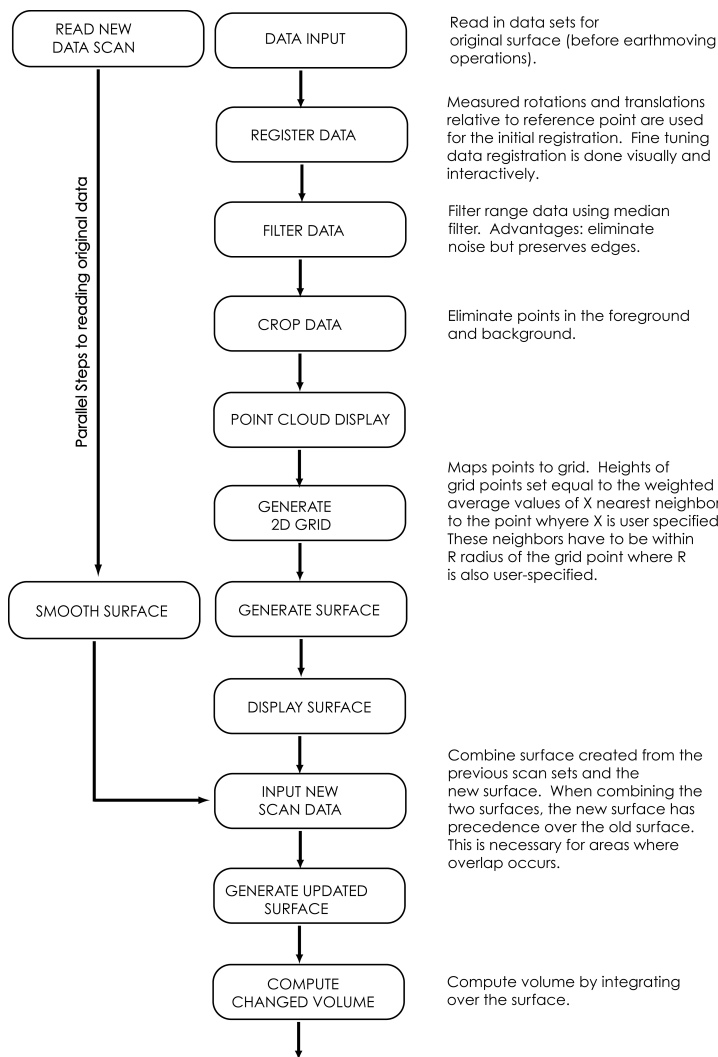


Figure 3: Flowchart for Open Data Explorer visual net program for post-processing of Lidar terrain data. This approach uses techniques for auto-gridding of scan data to a regular, rectangular mesh. The limitations of this approach are most easily recognized when scanning terrain with vertical walls as shown in Figure 7. More robust algorithms are being developed to handle vertical and undercut excavations.

where the volume calculations were performed and the new surface was regenerated and displayed. The data transmission, volume calculation, and surface regeneration were accomplished in a matter of seconds. The volume of sand removed was estimated at $0.15 \text{ m}^3 \pm 0.1 \text{ m}^3$ using a bucket of known volume. The computed cut volume, using Data Explorer was 0.168 m^3 . Major sources of difference between the estimated value and the computed values are compaction of the sand during removal from the sand pile and during placement of the sand into buckets. The estimated volume of sand removed was obtained by shoveling the sand into a bucket and calculating the volume of the bucket. Compaction of the sand would result in a lower estimated value of sand removed. Quantitative comparisons with different algorithms now being developed at NIST (Cheok et.al., 1999) indicated agreement on the calculated volumes.

scanner was placed above each of the points and the angles to the adjacent benchmarks were measured using the angle readout from the laser and a scope on the laser to sight to the adjacent points. In the future, the Lidar will be based on the survey rover (Figure 1) and GPS equipment will be used to determine the position and attitude of the laser scanner in real-time. The ultimate objective is on-the-fly Lidar registration at the construction site, as opposed to manual registration during post-processing. To this end, the data transmission from the laptop to the primary ATM backbone net was achieved by using a wireless Ethernet card in the laptop and a wireless Ethernet base station, operating at 1.5 Mbits/s. Figure 4f shows the acquired point cloud after registration of the four scans while Figure 4g shows the 3-D surface of the sand pile.

To simulate a change in the terrain, sand was removed from the pile using a front end loader. The volume removed was then automatically calculated as shown in Figure 5. Once the new Lidar data were acquired, the data file was sent wirelessly via FTP to the computer lab

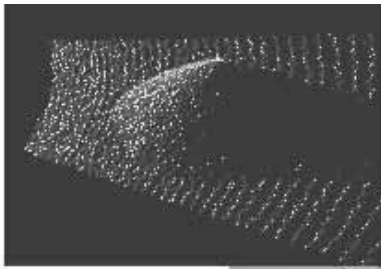


Figure 4a: north-west Lidar scan.

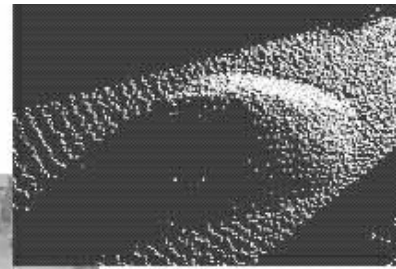


Figure 4b: northeast Lidar scan.



Figure 4c: south-west Lidar scan.



Figure 4d: southeast Lidar scan.

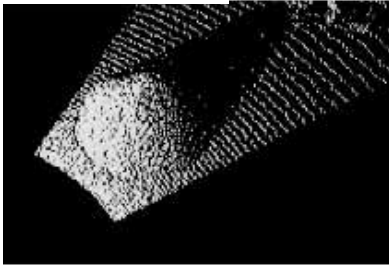


Figure 4e: The test sand pile in its original state.

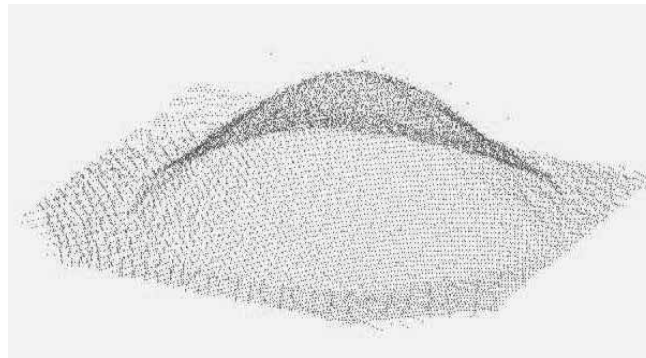


Figure 4f: Registered point cloud representing all four scans of the original sand pile.

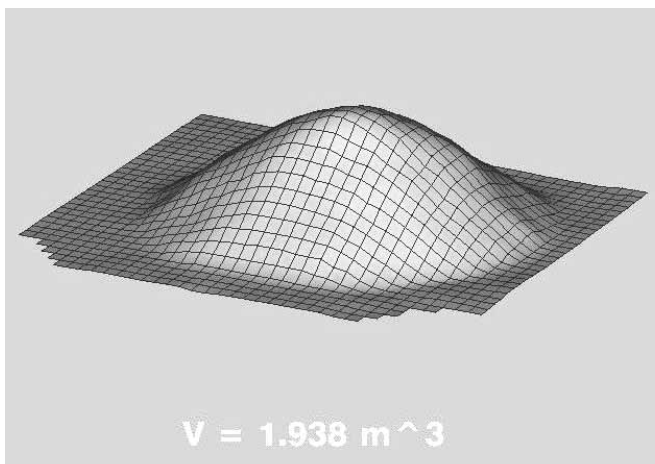


Figure 4g: 3D mesh resulting from gridding of data followed by smoothing to eliminate noise. Extraneous background scene data has been clipped to reduce the computational burden.

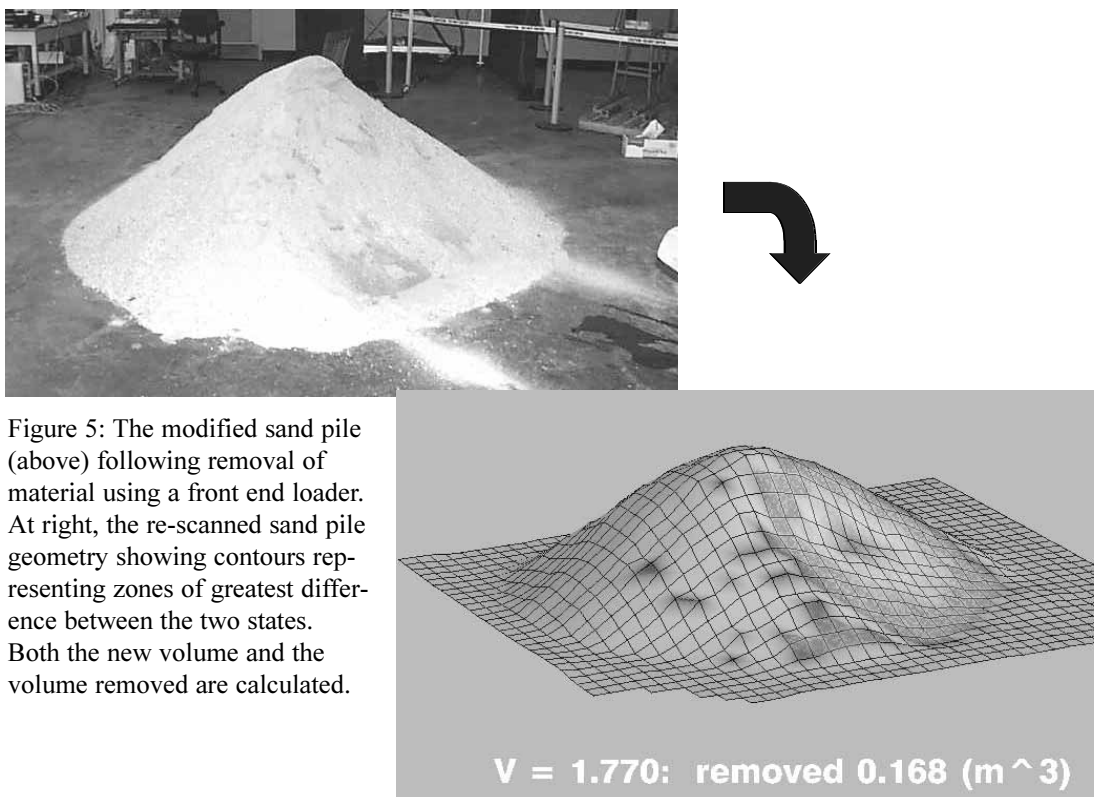


Figure 5: The modified sand pile (above) following removal of material using a front end loader. At right, the re-scanned sand pile geometry showing contours representing zones of greatest difference between the two states. Both the new volume and the volume removed are calculated.

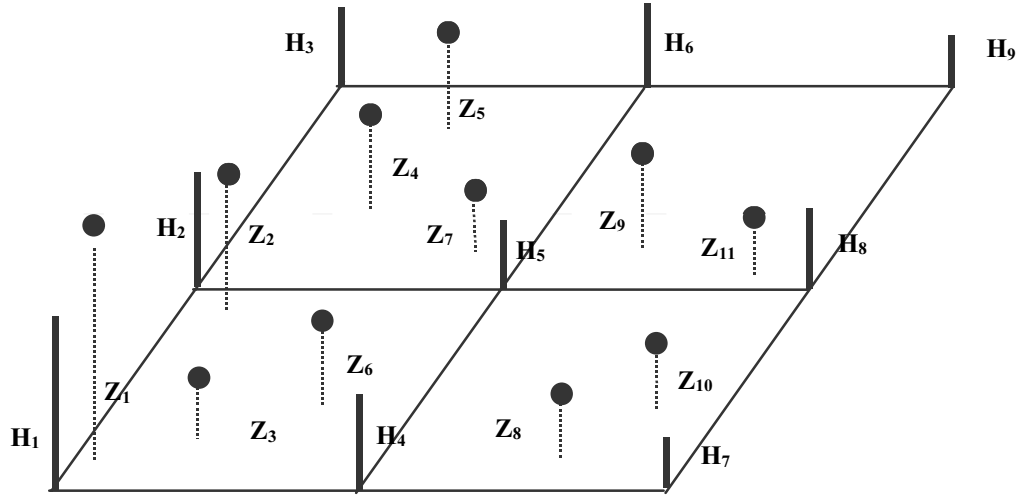
Data Visualization

The software package Data Explorer [OpenDX, 1999] was used to visualize the surface of the objects that were scanned by the Lidar. OpenDX, a previously proprietary program but now an open source code, is a general-purpose visual programming environment .

In the scenario described above, the terrain is scanned initially to define a reference surface. After this the geometry is changed by either removing or placing material at the excavation site (cutting and filling). The surface of the terrain object is visualized from the initial multiple scan data and recomputed from one or more updated scans -- however many are required to capture the new state. A general-purpose DX visual program was developed to handle scan data for scenes involving up to four reference (Lidar) locations (see Figures 4a,b,c, and d). The visual program reads in the Lidar data, registers the data, filters the data, maps a grid to the data, displays the surface defined by the grid, and computes the volume under the surface. A complete listing of the DX visual program and its associated macros may be found in [Cheok et.al., 1999].

At present the registration data, required for coordinate transformations, is user-defined in the DX source. Work is underway to make the code self-registering through the use of *REX* (the robotic excavation rover whose position and attitude are provided as a real-time source for Lidar data transformation prior to uplink). A general flow chart for the way in which Lidar terrain data is processed by the OpenDX routine is shown in Figure 3. The resulting visualization is displayed in Figures 4 and 5. The descriptive steps below cover those flow chart entries that are not obvious:

Data input: The files of XYZ data from the four initial laser scans for locations A, B, C, and D are read in (see Figure 4 a,b,c, and d, respectively). The XYZ data is also converted from the scanner coordinate system to the global coordinate system by switching the order of the Y and Z coordinates and the sign of the X coordinate.



$$H_i = \frac{1}{n} \sum \frac{Z_i}{r_i^a} \quad \text{Eq. (1)}$$

$$n = \sum \frac{1}{r_i^a}$$

Z_i = z - values of the data points

r = distance of data point to grid point

a = user specified integer

$$\text{Volume} = \text{Total Grid Area} \sum H_i$$

Figure 6: To map the XYZ cropped and combined point cloud data to the 2D grid, a weighted average of the Z values is taken. A diagram of this process is shown above. The Z values that are considered are within a certain radius of the grid point. Within the radius, the number of Z values can also be limited. Typically, the radius is the same size as an individual grid and the number of points to consider within that radius is set to 8. The weighting is an exponent on the radius and is typically set to 1. Once the heights are determined a surface can be displayed.

Register data: The three laser scan datasets (a, b, d) are registered (aligned) to the reference dataset, (c). The datasets are registered by applying a rotation and translation whose initial values are determined from the known location of the three datasets relative to the reference dataset. In the future this will be an automated procedure using the WGS-84 GPS coordinate system.

Filter data: The range data is smoothed by optionally applying a Gaussian or median filter. The median filter preserves sharp discontinuities while eliminating noisy data. To filter the range values of the laser scan data, the XYZ values are converted to a spherical coordinate system where the data is expressed as two angle values and one range value. The range value can then be filtered while the angle values remain constant. The filtered range value along with the constant angle values can then be converted back to XYZ values. Either a Gaussian filter or a median filter can be used. For the Gaussian filter, a filtered range value is computed by averaging itself with its neighboring values. For the median filter, a filtered range value is computed by ranking the neighboring values and itself in numerical order, then choosing the median value of the ranking. The median filter is much better at eliminating noisy, spurious data while preserving real discontinuities.

Crop data: The individual point cloud datasets are combined into one dataset and cropped to the area of interest before mapping a surface to it. Cropping eliminates unnecessary points in the foreground and background. The area of interest is set by minimum and maximum values of X and Y.

Point cloud display: To visually and interactively register the datasets, the XYZ scan data can be displayed as a point cloud or as a "raw grid". Any or all of the four datasets can be visualized as a point cloud, each with its own color.

Generate 2D grid: A regular uniform 2D grid is generated in the area of interest of the combined and cropped point cloud data. The 2D grid is used to map the point cloud data to a surface. The size of the 2D grid is determined by the X and Y extents of the cropped point cloud data and the size of an individual grid.

Generate surface: The point cloud data is mapped to the 2D grid to generate a surface. The height at a grid point is a weighted average of point cloud Z values. The weighting depends on the number of nearest neighbors within a radius around the grid point. The weighting, number of nearest neighbors, and radius are user-specified. See Figures 6 and 7 for the algorithm for and effects of this procedure.

Surface display: The surface is displayed along with the point cloud data. Several parameters can be set to change how the surface is drawn. A median filter can also be applied to the surface. The volume under the surface is also computed.

Input updated scan data: The file of XYZ data from any updated laser scans are read in. The new data is filtered, cropped, displayed similar to the initial laser scan data. The same 2D grid, from the initial laser scans, is used to map the updated point cloud data to its own surface.

Generate updated surface: The mapping to the 2D grid of updated laser scan point cloud data is substituted into the mapping from the initial combined laser scan data. This ensures that the updated surface will reflect the updated scan from the initial scans.

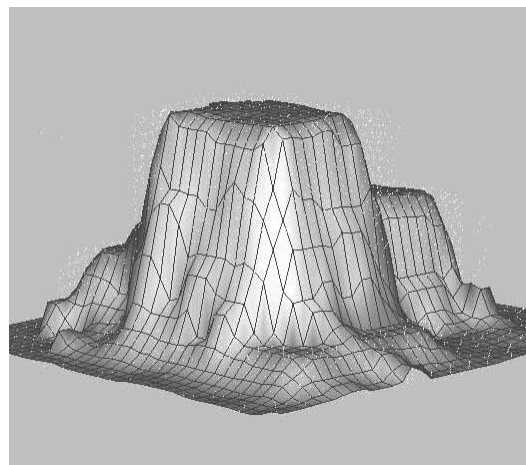


Figure 7: Current algorithm limitations: the gridding approach described in this paper requires the use of a uniform mesh to which unique elevation values are assigned. While this leads to simplified (fast) algorithm performance there are two situations where this will lead to quantifiable error: vertical excavation walls and undercuts. The effect is illustrated in the above two figures which show some angular “terrain” on the left and the lidar processed mesh on the right.

In future versions, the OpenDX code will serve as a waiting post-processor agent that acts upon the temporal project database each time a new time stamped data block becomes available. The output will be directed automatically to multiple consumers, as indicated in Figure 1.

Conclusions and Future Research:

An experimental 3D excavation status system has been developed at NIST for full-site Lidar scanning of earthmoving projects. Information about terrain changes in one location was sent via wireless Ethernet to another location for display and to perform cut/fill calculations. From these initial efforts, we anticipate the development of automated information transfer protocols for the uplink of both construction site terrain data as well as discrete component locations. This work is concurrently being conducted by other NIST researchers [Pfeffer, 1999]. Post-processing tools for data registration, display, and volume calculations were needed to achieve the results described herein and were developed in-house at NIST. Although the substantial OpenDX code developed for this project works impressively, it loses accuracy at vertical or undercut excavations due to its requirement to grid the raw point cloud data. Other, more robust, techniques, were developed in parallel and will be the subject of future papers. Initial work on these algorithms may be found in [Cheok et. al., 1999]. The present limitations of the data registration code will be eliminated in FY00 projects now underway to integrate the Lidar system with the robotic excavation status vehicle *REX*.

References

- Cheok, G.S., Lipman, R.L, Witzgall, C., Bernal, J., and Stone, W.C., (1999)** "NIST Construction Automation Program Report No. 4: Non-Intrusive Scanning Technology for Construction Status Determination," NISTIR-99-861.04-1 (in-print), National Institute of Standards and Technology, Gaithersburg, MD 20899, USA.
- Delaunay, B., (1934)** Sur la sphere vide, Bull. Acad. Sci. USSR (VII), Classe Sci. Mat., 793-800.
- Edelsbrunner, H., and Shah, N.R., (1996)**, Incremental topological flipping works for regular triangulations, *Algorithmica* 15(3), 223-241.
- FIATECH (1999)**, Brochure and video tape available from CII/FIATECH Consortium, c/o CII, 3208 Red River St, Suite 300, Austin, TX 78705-2697, <http://construction-institute.org>
- Krishna, M., and Bares, J. (1999)**, "Constructing Hydraulic Robot Models Using Memory-Based Learning," *ASCE Journal of Aerospace Engineering*, April 1999, pp. 34-42.
- OpenDX (1999)**, Open Source Software Project Based on IBM's Visualization Data Explorer, www.opendx.org
- Pfeffer, L. (1999)**, "Mobile Sensor Platform for Construction Metrology and Automation: Design and Initial Results," *Proceedings of the 16th International Symposium on Automation and Robotics in Construction (ISARC 16)*, Madrid, Spain, September 22-24, 1999.
- Riegl (1999)**, LPM98-VHS Laser Profile Measuring System 98 - User's Manual, Austria, 58 pp.
- Sackos, J. T, Bradley, B. D., Diegert, C. F., Ma, P. W., Gary, C., (1996)**, "Scannerless Terrain Mapper," *Proceedings of the SPIE/International Society for Optical Engineering conference on Spacecraft Control and Tracking in the New Millennium*, Aug. 6, 1996, Vol. 2810, pp. 144-153.